Materials & Design 219 (2022) 110753

Contents lists available at ScienceDirect

Materials & Design

journal homepage: www.elsevier.com/locate/matdes

In-situ analysis of the thermoelastic effect and its relation to the onset of yielding of low carbon steel

Simon Vitzthum [a,*], Joana Rebelo Kornmeier [b], Michael Hofmann [b], Maximilian Gruber [a], Emad Maawad [c], António C. Batista [d], Christoph Hartmann [a], Wolfram Volk [a]

[a] Chair of Metal Forming and Casting, Technical University of Munich, Garching near Munich, Germany
[b] Heinz Maier-Leibnitz Zentrum (MLZ), Technical University of Munich, Garching near Munich, Germany
[c] Helmholtz-Zentrum Hereon, Institute of Materials Physics, Geesthacht, Germany
[d] University of Coimbra, CFisUC, Department of Physics, Coimbra, Portugal

HIGHLIGHTS

- The thermoelastic effect is analyzed on micro level and its potential for material characterization is shown.
- In-situ synchrotron diffraction experiments with time synchronous temperature measurement are performed.
- Extensive results on the relationship between lattice strains as well as dislocation densities and the specimen temperature behavior.
- Introduction of two new temperature-dependent elasticity parameters and a clear determination method for the elastic loading modulus.

GRAPHICAL ABSTRACT

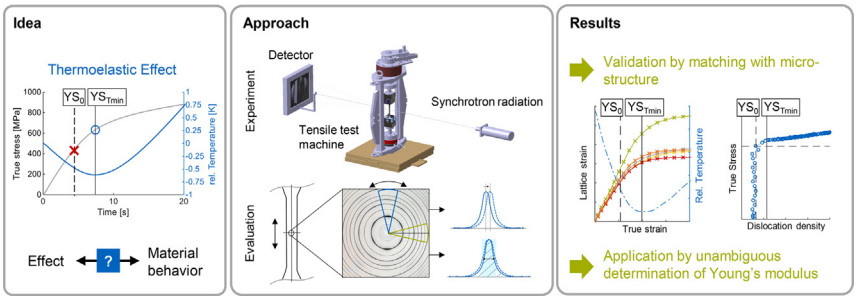

ARTICLE INFO

Article history:
Received 10 March 2022
Revised 10 May 2022
Accepted 12 May 2022
Available online 16 May 2022

Keywords:
Elasticity
In-situ analysis
Synchrotron radiation
Young's modulus
Tensile test
High strength steel

ABSTRACT

The thermoelastic effect indicates the dependency of temperature and volume change in the material and, due to the heat released during plastic deformation, a temperature minimum occurs in the region of the onset of yielding. An experimental setup is presented for the microscopic analysis of the thermoelastic effect, which allows high precision measurements of specimen. In-situ diffraction experiments were performed for a single phase low carbon steel HC260Y using synchrotron diffraction at the High Energy Material Science beamline P07 in Petra III, DESY. This allows a direct comparison of the onset of yielding by observing the evolution of lattice strains and dislocations densities with the specimen temperature in a continuous cyclic test having high measuring frequency and accuracy. Therefore, the lattice strains are evaluated based on the peak shift of several lattice planes and the dislocation density is estimated based on the micro strain due to peak broadening. The results prove existing assumptions about the relation between the thermoelastic effect and the onset of yielding and clearly qualify the temperature-based determination method for material characterization on a microstructural basis. The usefulness of the temperature elasticity parameters is shown exemplarily with the determination of loading moduli and compared to existing methods.

* Corresponding author.
E-mail address: simon.vitzthum@utg.de (S. Vitzthum).

https://doi.org/10.1016/j.matdes.2022.110753
0264-1275/

1. Introduction

The increasing use of high-strength steels and the development of even stronger steels make precise prediction of springback more difficult and at the same time more important [1,2]. That is why precise material parameters describing the elastic behavior are crucial for modelling springback [3,4]. In theory, there is elastic deformation up to a certain stress value at which elastic–plastic deformation starts [5]. Based on this, the onset of yielding is described by the deviation of the stress–strain curve from its initial linear slope [6]. Unless this critical value is reached, the deformation should be mechanically and thermodynamically reversible, i.e. the specimen returns to its initial geometry and virtually no deformation work is released [7]. In reality, elastic deformation shows nonlinear [8] and even anelastic behavior [9,10]. In any case the question now arises of how the critical value of the onset of yielding can be determined precisely. The most widely used method is an empirical approach, in which the deviation from linearity of the stress–strain curve is determined and an equivalent yield strength is found [11]. For this, the yield strength at 0.2 % plastic deformation is the one most commonly used. If one looks into the prescribed procedure by the standards [12,13], it is found that this determination has some limitations. For the determination, a parallel line to the linear initial slope is shifted to the respective plastic strain, in order to read off the associated stress value [14]. However, especially mild steels show a very smooth elastic–plastic transition and almost no linear region. Thus, the determination of the initial slope is not clearly apparent and strongly depends on the chosen limits [15]. This results in a highly user-dependent evaluation method with no real link between the parameter and the physical behavior of the material.

An overview of several approaches to determine the onset of yielding is given in [16]. Included are temperature-dependent ones, based on the findings of Weber [17] in 1830 and especially Joule and Thomson, who showed that their insights on the volume-dependent temperature change are also valid for solids, more specifically metallic materials [18,19]. This phenomena is well known as the thermoelastic effect [20,21]. Due to the Poisson ratio of around 0.3 for steel [22], the volume increases during elastic elongation, which leads to a decrease in temperature. Since the energy released by plastic deformation is to a large extent converted to heat [23–25], the temperature increases during plastic deformation. In addition to the original experimental confirmation of these findings by Compton and Webster, in 1915 [26], several studies around this topic were published more recently [27–29] with an comprehensive overview and detailed descriptions given in [30]. Due to the small temperature differences for metallic materials (<1 K), the measurement technology was initially the limiting factor [31]. Belgen was the first to use an infrared camera to measure the effect [32], and in [31] miniature sensitive thermistors were used to detect the temperature. Using those, it was possible to measure a temperature minimum with a relative temperature change of 0.35 K for a mild carbon steel. In the following, results were published for austenitic steel, titanium and aluminum alloy [33,34], as well as for stainless steel [35–37] and low carbon steel [38]. Jocham et al. [39] used welded-on thermocouples and showed results for biaxial experiments with a mild steel. In [40] a clip-on device, based on the findings of [11], is presented with an integrated PT1000 sensor for temperature measurement.

In the meantime, in-situ diffraction experiments have evolved further and high resolution continuous experiments are used to gain insight into microstructural behavior [41–43]. Also, measurement technology has improved and high-precision temperature measurements are possible. However, the key question is which state in the material the temperature minimum really describes. First assumptions have already been made in [40], but since these are based on explanations in the microstructure, studies of the microstructure are necessary. In this study, an experimental setup is presented, which allows the correlation of macroscopic and microscopic material values. The focus is on matching the thermoelastic effect with the microscopic behavior of the material, in order to clarify the significance of the temperature minimum regarding the onset of yielding. For this purpose lattice strains are determined in a synchrotron diffraction measurement for the material HC260Y. Additionally, dislocation densities are evaluated for the single phase steel and compared with the temperature behavior. In this way, the relationship between the temperature minimum and the material behavior can be experimentally classified. The results support the statements made in the preliminary work [40]. The determination of Young's modulus is an excellent example showcasing the potential of using the thermoelastic effect for material characterization. It is a key parameter in describing the elastic material behavior and its determination is complex. It is highly dependent on the chosen determination approach and especially on the boundaries for the linear fit [44]. The additional temperature elasticity parameters could be used to introduce more robust methods for the elastic modulus determination. Therefore, one possible application for the determination of a loading modulus is shown within this study. In general, the objective is to better understand material behavior, and especially the yielding of sheet metals. This is to provide a basis for the improvement of existing material models in order to increase their prediction accuracy. These models, although phenomenological-based, are important in the field of material modelling [45].

2. Theory

2.1. Thermomechanical basics

Basically, a standard tensile test is a non-isothermal experiment. The temperature change that occurs is based on complex thermodynamic relationships in the material. For this reason, a purely mechanical description of the elasticity is not fully comprehensive. The temperature change was described by Bottani and Caglioti [11] and follows [46]. In the pure elastic range, the thermodynamic state of a material is stable, having virtually no change in entropy. The material state is close to equilibrium and dislocations are immobile. This state can be described using the strain tensor and the prevailing temperature. New formation and migration of dislocations lead to a change in the dislocation density. This change disturbs the equilibrium, since it must be considered as an additional thermodynamic variable. Hence, the onset of plastic yielding, where this occurs, is the point of time at which it is no longer possible to describe the thermodynamic state by conventional terms. [47].

The cooling of metallic materials leads to volume contraction. Conversely, an increase in volume leads to cooling. During linear elastic deformation the volume can be expressed with Eq. (1).

$$\frac{\Delta V}{V_0} = (1 - 2\upsilon)\varepsilon_l \tag{1}$$

where V_0 is the initial volume, ν is Poisson's ratio and ε_l is the longitudinal strain. Thus, the volume is increasing during elastic elongation. During elastic deformation, the relationship between the temperature change ΔT and the initial temperature T_0 can be deduced from Eq. (2) using Maxwell's relation [31].

$$\frac{\Delta T}{T_0} = -\gamma(1 - 2\upsilon)\varepsilon_l \tag{2}$$

Here γ is the Grüneisen parameter, which is described by the thermal expansion coefficient, the isothermal compressibility and the specific heat capacity at constant volume [31]. Since it is

complex to determine the Grüneisen parameter experimentally, another derivation has proven useful to describe the thermoelastic effect, which is based on Heinz's generalized thermoelasticity model [48] and is shown in [31]. Finally, after derivation one comes to the following equation (3) proposed by W. Thomson [18].

$$\Delta T = -\frac{\alpha T_0 \Delta\sigma}{C} \tag{3}$$

where T_0 is the initial specimen temperature, α the linear coefficient of thermal expansion, σ the stress and C the heat capacity [49]. Consequently, materials with a positive expansion show a decrease in temperature during adiabatic elastic tension and an increase during adiabatic elastic compression. The calculations based on this theory showed reasonable results in comparison with experimental data for various materials, such as ceramics, polymers, metals, alloys and composites [50].

2.2. Temperature-determined onset of yielding

In [40], the assumption was made that during purely elastic loading, the temperature signal is linearly decreasing. Consequently, a deviation of the temperature behavior from linearity means that plastic deformation sets in. In the following, this idea will be described in detail. For this purpose, the onset of yielding is divided into three phases as a function of temperature (see Fig. 1). The respective limits are represented by the parameters YS_0 and YS_{Tmin}. In the first elastic phase, reversible deformation takes place. The crystal lattices are stretched, but no lattice defects are formed [51]. Hence, in a diffraction experiment, the measured elastic lattice strains are increasing rapidly during this phase whereas there is no increase expected for the dislocation density. The stress–strain curve increases linearly while the temperature decreases linearly. At a certain point the temperature curve deviates from linearity, which can be determined by the method introduced in [40], which is further improved in the current study. The deviation from linearity implies that the sample is heated by slight plastic deformation, but this heating is still less than the elastic cooling. The elastic deformation is therefore still predominant. This point of deviation from linearity is assumed to be the onset of yielding and that is why it is called yield stress at zero plastic strain (YS_0) here. It is the start of phase 2, the onset of yielding phase. During this phase crystal lattices start to yield separately dependent on their stiffness, which lead to more heat dissipation. Finally, the temperature increase because of plastic deformation and the decrease because of elastic deformation are in equilibrium. This state can be characterized by the temperature minimum, which is denoted as the parameter yield stress at temperature minimum (YS_{Tmin}). In the elastic–plastic deformation phase the temperature rises again and approaches a linear behavior. In summary, it is assumed that the onset of plastic deformation starts before the minimum, but that the minimum describes the point in time from which the plastic deformation is decisive. The objective of this study is to investigate this assumption also on the micro scale level.

The procedure to determine the parameter YS_0 is similar to the one shown in [40], but is improved in terms of robustness. Fig. 2 (a) shows the true stress versus time and corresponding temperature versus time curve for the material HC260Y, which were recorded with the experimental setup described in more detail in Section 4, with a strain rate of $1.5 \times 10^{-4}\ s^{-1}$. The initial loading and the first unloading-loading cycle are shown. Looking at the temperature curve it can be seen that during elastic loading (el), elastic–plastic loading (pl) and elastic unloading (eul) the slopes are approximately linear. This is confirmed by the temperature gradient curve in Fig. 2 (b), as the horizontal course of the first derivative describes linear behavior. For the temperature gradient, the simple approach of finite differences was chosen to change the data as little as possible. This results in the significantly larger noise of the temperature derivative compared to the temperature curve. However, by averaging through the linear line fits, the influence on the evaluation is negligible. The first derivative allows straightforward determination of the transitions in the temperature. Therefore, two regression lines have to be found [52] (yellow lines). For the horizontal fit, the green marked values are used. For the vertical fit the gradient values marked in blue from the temperature minimum backwards are taken. The number of data points for the regression depends on the measurement frequency. The point of time of the intersection leads to the parameter YS_0 via an angle bisector on the data curve. In Fig. 2, it must be noted that the axes are strongly scaled for better representation and the bisector of the angle is virtually equal to the perpendicular in this case. It can be seen that determination of the parameters for the second loading is even clearer, which is analogue for all consecutive loadings (see Fig. 2 (b)).

During the tests, the following data were recorded synchronously in time: macroscopic strain and stress, temperature, as well as lattice strain and dislocation densities (see Section 5). This time-synchronous detection of all data makes it possible to link the parameters YS_0 and YS_{Tmin} directly to the microscopic data from the diffraction experiment.

3. Material

Low carbon interstitial free steel HC260Y with a sheet thickness of 1 mm is considered in this study. The single phased, ferritic HC260Y is a widely used deep drawing steel with high formability

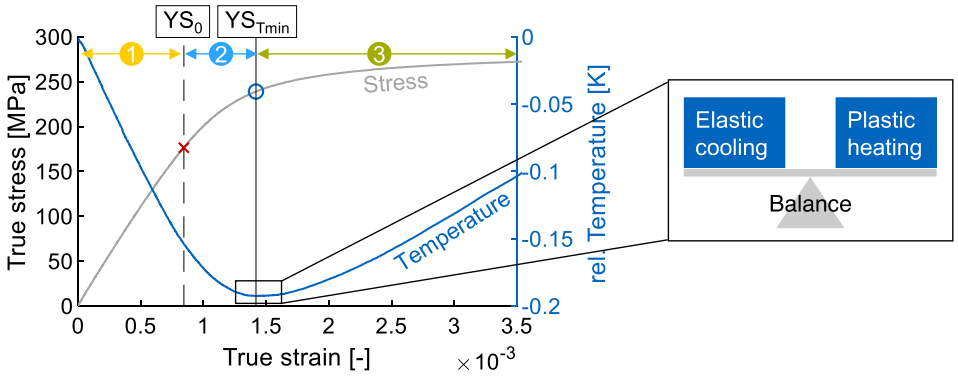

Fig. 1. True stress versus true strain and corresponding temperature versus true strain curve (HC260Y). Classification of the onset of yielding in three phases by the parameters YS_0 and YS_{Tmin}.

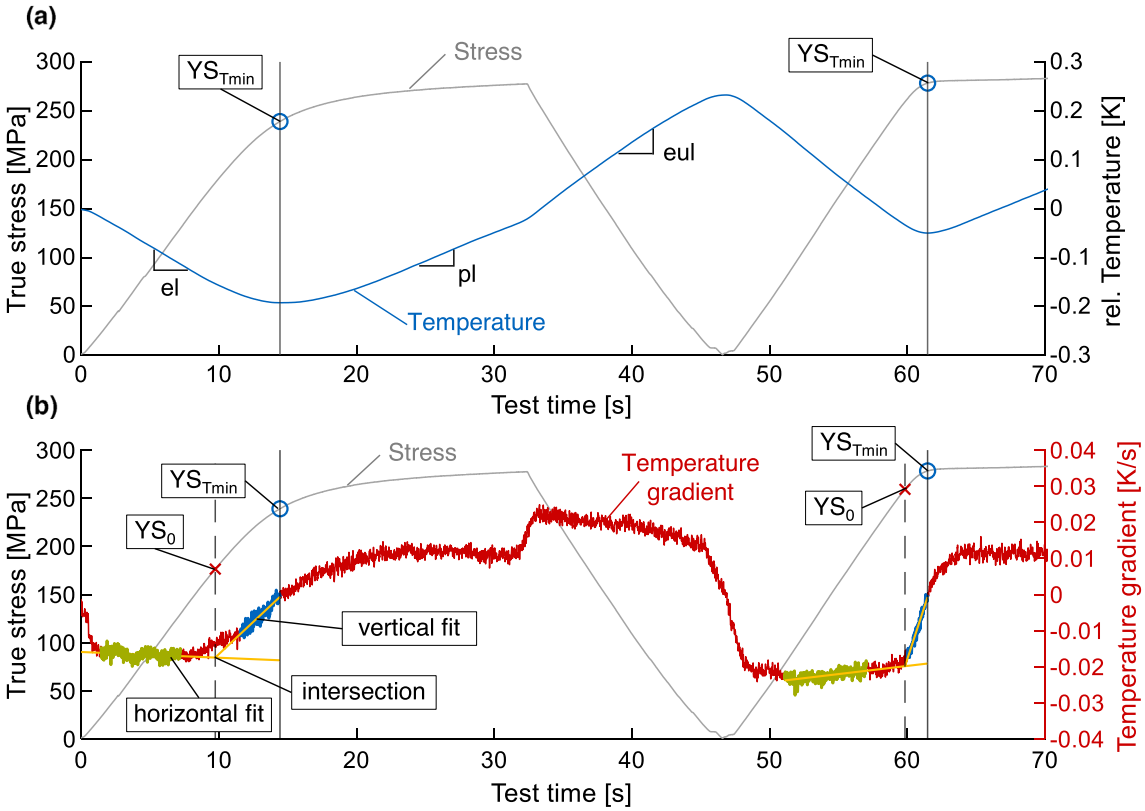

Fig. 2. Initial loading and first unloading-loading cycle (HC260Y, strain rate 0.00015 1/s) for (a) stress – relative temperature versus time and (b) temperature gradient - relative temperature versus time; Yield stress at temperature minimum (YS_{Tmin}) and yield stress with temperature gradient evaluation method (YS_0) are marked.

and yet relatively high yield strength, often used for complex inner or outer car body panels. It has a yield strength at 0.2 % plastic strain of 292 MPa and a tensile strength of 425 MPa. The microstructure of the material is depicted in Fig. 3 (a). In comparison to a ferritic-martensitic dual phase steel for example, the HC260Y steel sample is rather coarse-grained (mean grain size around below 20 µm). The chemical compositions of the materials determined by Optical Emission Spectrometer (OES) are shown in Table 1.

Cyclic tensile tests were performed within this study for investigation. For this purpose the specimen geometry was used according to the German standard (DIN EN ISO 50152, Form H). It has a parallel length of 75 mm, width of 12.5 mm and thickness of 1 mm (see Fig. 3 (b)). The initial marked length is 50 mm. This geometry is used for all tests within this study. All specimens were tested in the rolling direction.

4. Experimental setup

Microscopic in-situ synchrotron diffraction experiments are performed to also extract information on a microscopic scale. From the diffraction data, lattice strains and dislocation densities for the purely ferritic HC260Y were evaluated for micro analysis. The experiment was performed at the High Energy Materials Science beamline HEMS, P07B, of Helmholz-Zentrum Hereon at PETRA III (DESY, Hamburg). The high-energy x-ray beam was monochromatized by a single bounce monochromator (SBM) with a flat water-

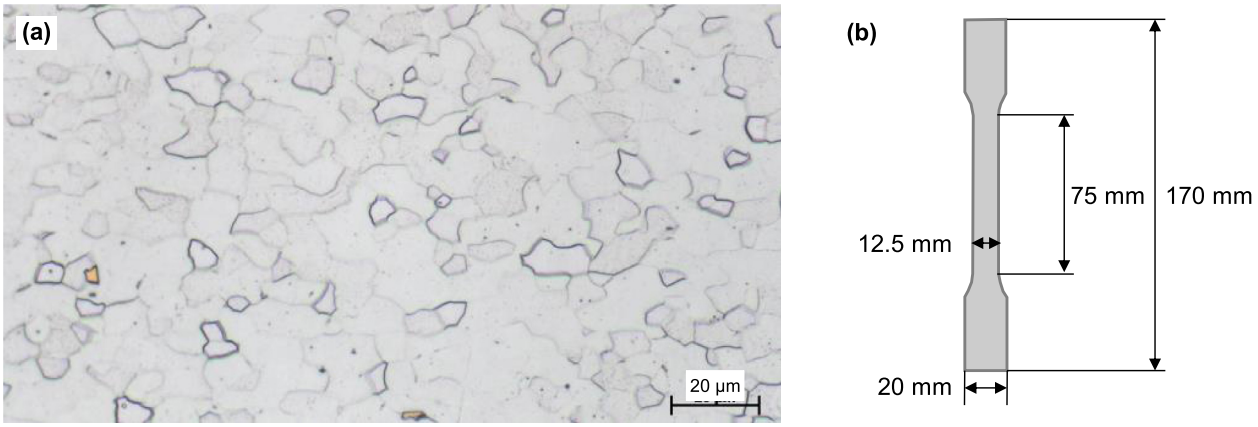

Fig. 3. (a) Microstructure of the purely ferritic HC260Y; (b) Specimen geometry for tensile tests.

Table 1
Chemical composition of the materials in [%] - mass fractions.

	C	Si	Mn	P	S	Al	Ti	Nb
HC260Y	0.004	0.123	0.770	0.063	0.007	0.046	0.046	0.030

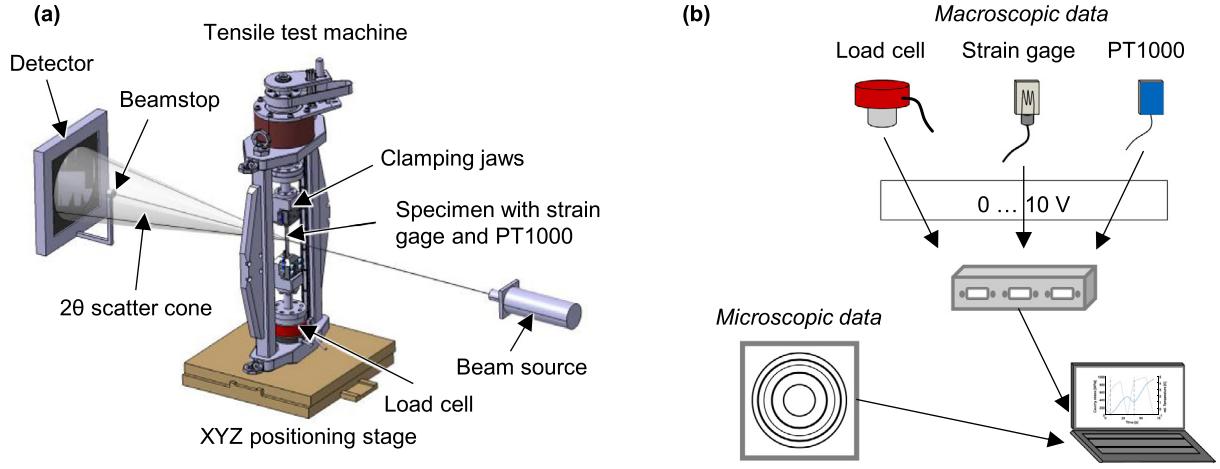

Fig. 4. (a) Test setup for in-situ synchrotron measurement at HEMS (DESY, Hamburg); (b) Schematic representation of the measurement data acquisition.

cooled Laue crystal Si (220), set to achieve a wavelength of 0.14235 Å. The beam size was 0.7 × 0.7 mm2.

Fig. 4 (a) shows the sketch of the beam line setup with the mounted tensile rig on two linear displacement stages (horizontal and vertical). A Perkin Elmer XRD 1621 flat panel was used for fast data collecting, having 2048 × 2048 pixels with a pixel size of 200 × 200 μm^2. With a specimen to detector distance of 1062 mm, six complete Debye-Scherrer rings could be obtained per second. Between 1700 and 2500 diffraction patterns were measured during the cyclic tensile test along the load–elongation curve. The misalignment and the distance to the sample from detector was calibrated using Fit2d software with a standard Lanthanhexaborid (LaB_6) powder with 1 mm thickness to match approximately the specimen thickness [53].

The specimen was mounted in a test rig dedicated for diffraction experiments [54]. Special clamping jaws having as little clearance as possible were developed to ensure accurate measurement during the loading and unloading cycles. Hardened, high friction clamping inserts prevent the specimen from slipping. The macroscopic strain was measured using special high-elongation strain gages (KYOWA KFEM-5–120-C1). The load is recorded via a load cell, which is installed in the test machine. Platinum-based resistance thermometers (PT1000, precision class B) measure the specimen temperature. The PT1000 sensor is applied to the specimen by a commercially available clamp and connected to the data acquisition system HBM QuantumX. The load and displacement signals of the tensile test machine are also transferred to the HBM QuantumX, to get synchronized data and prevent a measuring error due to triggering. All 0–10 V measuring channels are finally converted to the respective physical units. The data acquisition system is triggered to the microscopic synchrotron measurement, ensuring that all data is synchronized (Fig. 4 (b)). The measuring frequency of the macroscopic data is 10 Hz and the frequency of the microscopic diffraction data is 1 Hz, which is reasonable for this kind of experiment. With this test setup, a standard deviation of 2 MPa for YS_{Tmin} can be achieved as shown in a series of cyclic tensile tests with a homogeneous mild steel (DC06) performed in the laboratory before the synchrotron measurements.

During the tensile tests only the temperature difference (relative temperature) between the current temperature T and the initial temperature T_0 of the specimen is measured, as this dispenses with an otherwise complicated calibration of the absolute temperature. Hence, all temperature curves shown in the following indicate $\Delta T = T\text{-}T_0$. The temperature in the beam line housing is kept constant at a temperature of 20 °C throughout the measurements by an air conditioning system. After inserting the specimen and attaching the sensor, a 10 min waiting period takes place for the temperature signal to stabilize. The specimen was loaded and unloaded using position control to 1.5 mm travel of the crosshead and then in 3 mm steps until around 15 % engineering strain, while continuously recording diffraction data. The strain rate was set to 0.00015 s^{-1}. To guarantee precise local measurement, the XYZ position stage with the tensile test machine was moved in the opposite tensile direction at half speed.

5. Evaluation methods

An area detector image with the Debye-Scherrer rings and the corresponding integrated 1D-diffraction pattern is shown in Fig. 5 for the unloaded state. Crystallographic parameters of the measured materials, like lattice strains on basis of d-spacing values, the crystallographic texture and dislocation information on basis of micro strain broadening could be obtained from the diffraction data. In order to extract the information on the grains oriented in the loading (LD) and transversal direction (TD), a sector of ± 10° along the specific directions of the complete Debye–Scherrer ring are integrated using Fit2d software (Fig. 5).

This generates a diffraction profile for each individual measurement and thus the profile evolution during the cyclic tensile test can be evaluated by using an appropriate peak shape function. The lattice spacing d_{hkl} for the diffraction profiles at the specific $2\theta_{hkl}$ angles for the (hkl) lattice planes (200), (211), (220) and (310) is calculated using Bragg's law (equation (4)) [55].

$$n\lambda = 2d_{hkl}sin\theta_{hkl} \tag{4}$$

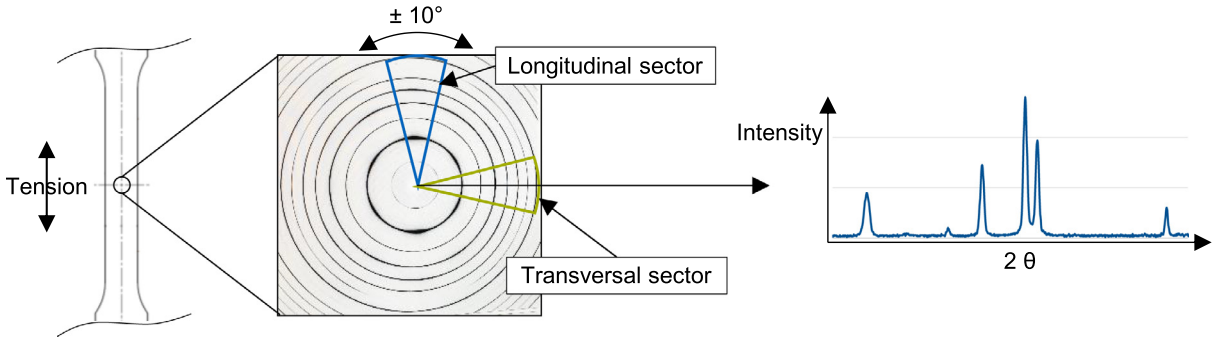

Fig. 5. Schematic diagram for the evaluation of the microscopic X-ray data.

The lattice strain ε_{hkl} can be calculated from the measured lattice spacing d_{hkl}, as the ratio between the change of the lattice distance due to the loading and the initial distance (equation (5)) [56,57].

$$\varepsilon_{hkl} = \frac{d_{hkl} - d^0_{hkl}}{d^0_{hkl}} \tag{5}$$

For evaluating the elastic strains from the d-spacing, the respective values at initial state (load of 0 MPa) were taken as reference.

With regard to the onset of yielding, besides the peak shift additional information can be extracted from the diffraction peak shape profiles. Frequently used to evaluate peak broadening are integral breadth (IB) methods [58]. These are particularly suitable when trends in the microstructural behavior are of interest and should be compared during an experiment [59]. The broadening of a Bragg reflection peak contains besides the instrumental resolution also effects due micro strain, or distortion and crystallite size [60]. The Williamson-Hall method allows to separate the broadening due to size-effects and to micro strains by bringing the peak broadening into relation with the 2θ angle [61]. The elastic anisotropy of the alpha ferrite under consideration is not taken into account in the classical Williamson-Hall method in contrast to the modified method [62]. For the following reasons, the more complex modified method was not used in this study. First, an additional analysis of the type of dislocation, which is possible via the contrast factor of the modified method [62], is not the aim of the present study. The objective is to match the general dislocation formation with the parameters YS_0 and YS_{Tmin}, so that the correlation with the onset of yielding can be investigated. On the other hand, mainly lattice planes of higher order are affected by elastically anisotropic behavior [63]. However, since the lattice plane (310) showed essentially linear behavior in the WH plot even at high strains (see Fig. 7 a), the classical method was considered sufficient. For the chosen method, the IBs of the specimen in question have to be corrected by the instrumental resolution. For this, Lanthanhexaborid (LaB6) powder matching the specimen thickness (1 mm) was measured and the IBs of the considered lattice planes were corrected with the corresponding LaB6 IBs. Fig. 6 exemplary shows the peak profile for the lattice plane (211). Represented is a Gaussian fit for the initial condition at 0 MPa with associated measurement points, as well as after the 6th loading (also at 0 MPa). Furthermore, the dashed line is the fit for LaB6, which is assumed to represent the instrumental resolution. For comparison the LaB6 peak has been shifted to the (211) peak position and the intensity is normalized. It is noteworthy that the difference of the peak for the initial state at 0 MPa and the instrumental resolution is negligible. However, at the 6th loading, a clear broadening is visible. Furthermore, it is apparent that using a Gaussian peak profile, an excellent agreement between fit and measurement points is achieved.

Using a Gaussian fit, the integral breadth β is composed as follows [64].

$$\beta^2 = \beta^2_{size} + \beta^2_{strain} + \beta^2_{instrument} \tag{6}$$

For validity reasons, also a Voigt function, i.e. a convolution of a Lorentzian and Gaussian peak shape function, was used for the fits. However, the results showed essentially no Lorentzian contribution was found for the peak profile and the goodness of the fit was equal to that of a pure Gaussian fit. Therefore, it is assumed that a Gaussian fit was sufficient to describe the evolution of the peak broadening of the samples measured here.

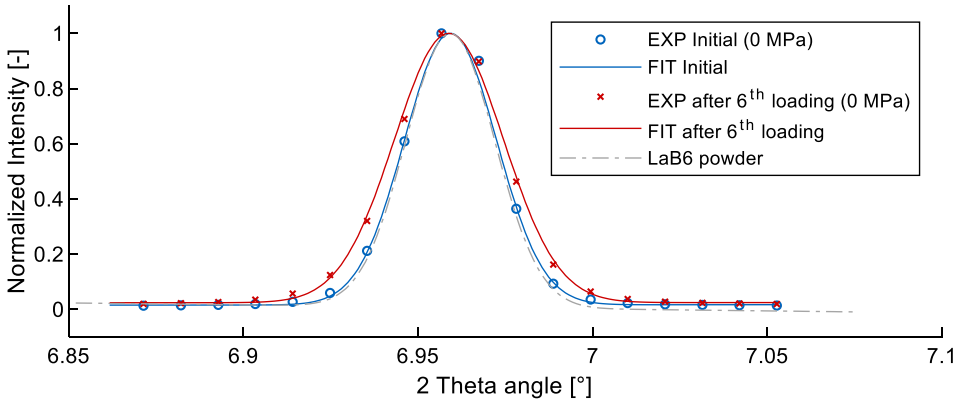

Fig. 6. (211) - profile peak and its Gaussian fit for the initial material (at 0 MPa) and the prestrained material after 6 loadings (at 0 MPa). The corresponding LaB6 peak (dashed line) is fitted in the (211) peak to see the instrumental resolution. The intensities are normalized.

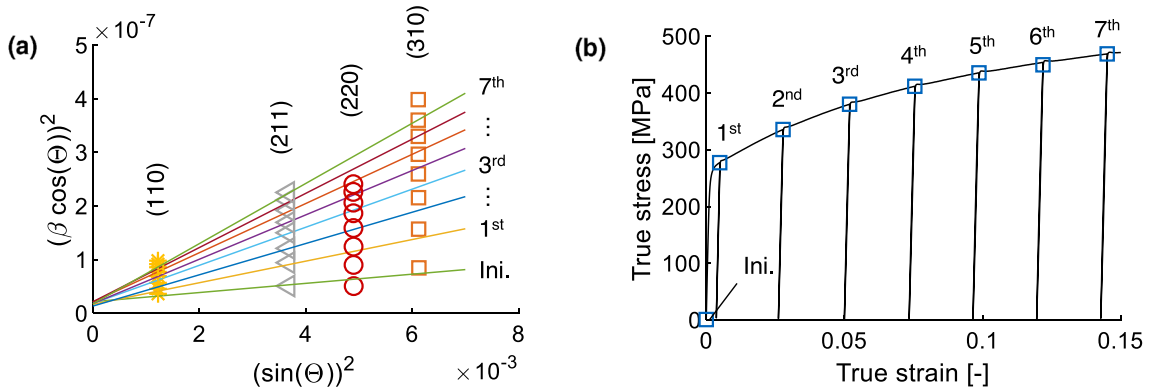

Fig. 7. (a) Williamson-Hall plot for four lattice planes for the stress states shown in (b).

On basis of IBs for at least two lattice planes of different orders, a root mean square strain $\langle \varepsilon^2 \rangle^{1/2}$ (RMS) can be determined by a Williamson-Hall plot [65,66]. The Williamson-Hall equation for the real space and a pure Gaussian fit results in.

$$(\beta cos\theta)^2 = \frac{\lambda^2}{D^2} + 16 \cdot e^2 \cdot (sin\theta)^2 \tag{7}$$

where λ is the wavelength, D is the crystallite size and θ the Bragg angle. The RMS is related to the micro strain e as $\langle \varepsilon^2 \rangle^{1/2} = (2/\pi)^{1/2} \cdot e$ [67]. As Equation (7) is a linear function when plotting $(\beta \cos\theta)^2$ versus $(\sin\theta)^2$, the RMS can be extracted from the slope, while the crystallite size can be determined by the intercept of the linear function. Fig. 7 (a) shows the Williamson-Hall plot for the stress states shown in Fig. 7 (b). The linear regression was calculated using the four Bragg reflections (110), (211), (220) and (310), respectively. The regression lines pass close through the origin, which indicates that size-effects can be neglected and thus, the peak broadening is mainly caused by micro strains and hence, dislocations [68].

The RMS were determined for each diffraction measurement in the described way and dislocation densities were estimated by using the Williamson-Smallman dislocation model, as described by the following equation [69].

$$\rho = \frac{K^2 \cdot \langle \varepsilon^2 \rangle}{D \cdot b^2} \tag{8}$$

In this equation K is a constant ($K = 6\pi$) and b is the burgers vector for the considered slip system, in this case ⟨111⟩ direction. D is the coherent domain size, but as already stated, it is assumed that there are no size-effects. According to Williamson and Smallman [69] it is valid, for the simplest evaluation of the dislocation density to assume $D = 1$.

6. Results

The experimental setting allowed in-situ synchrotron diffraction measurements with high resolution and synchronous temperature measurement on the same specimen to investigate the link between the thermoelastic effect and the onset of yielding. Accordingly, the recorded diffraction data can be directly compared to the temperature and the macroscopic stress and strain. This makes it possible to link the micro structural state during yielding to the temperature minimum and YS_{Tmin}, respectively. In addition, the usefulness of the parameter YS_0 can be validated. The determination of YS_{Tmin} and YS_0 is shown in Section 2.2 and is analogue for all further loading cycles. Four lattice strains longitudinal and transversal to the loading direction are evaluated in parallel for the material HC260Y within this study.

6.1. Lattice strains

Fig. 8 shows the lattice strain versus true macroscopic strain for the lattice planes (200), (211), (310) and (220) for the initial loading in the longitudinal and transversal direction (HC260Y). Each circle in the figure represents a synchrotron data point. The measured d-spacing values at the beginning were used as reference values for the lattice strain evaluation. The figure illustrates when the individual grains with the corresponding lattice planes oriented in either the loading or transversal direction plasticize. In diffraction experiments, only elastic strain leads to a measurable peak shift of the Bragg reflection. After the slip system is activated for a grain oriented in the corresponding load direction, i.e. the onset of yielding, no further peak shift can be detected and thus no further linear increase in lattice strain is observed. In Fig. 8, correspondingly the grain is fully plastically deformed when the lattice strain curve approaches a horizontal one [60]. The blue line in the same figure represents the relative temperature curve with the two parameters YS_{Tmin} and YS_0 (vertical lines) were determined from this, as described above.

The (211) and (220) planes show similar behavior, the (310) plane behavior differs slightly and the (200) plane show significant different behavior, as to be expected. In both, longitudinal and transversal directions the (200) plane is the most compliant and has the lowest diffraction elastic constant (DEC), which is both in good agreement with the results in [70], confirming the assumption of the (200) plane being more elastic. Furthermore, all lattice planes show a smooth transition from the linearly increasing strain in the beginning to the approximate horizontal behavior for both loading directions. The blue temperature line also shows this smooth transition. Note that at the temperature minimum there is a rather flattened region before the temperature increases again. Little plastic work is necessary to elongate the HC260Y. Thus, the dissipated heat is also low, and the temperature increases slowly. When the temperature increases again, the negligible Bragg peak shifts indicate almost no increase in lattice strain. Accordingly, it can be concluded that at this point all lattice planes are in the plastic range. This behavior is seen for the longitudinal as well as for the transversal direction.

Fig. 9 shows lattice strain versus true macroscopic strain curves for further loadings of the cyclic tensile test. The 3rd, 6th and 8th loading are presented, which are at true strains of around 3 %, 9 % and 15 %. Again, the (200) lattice plane clearly shows the steepest slope in the elastic range, which is equivalent to the lowest DEC. The behavior of the planes approaches a horizontal. Fur-

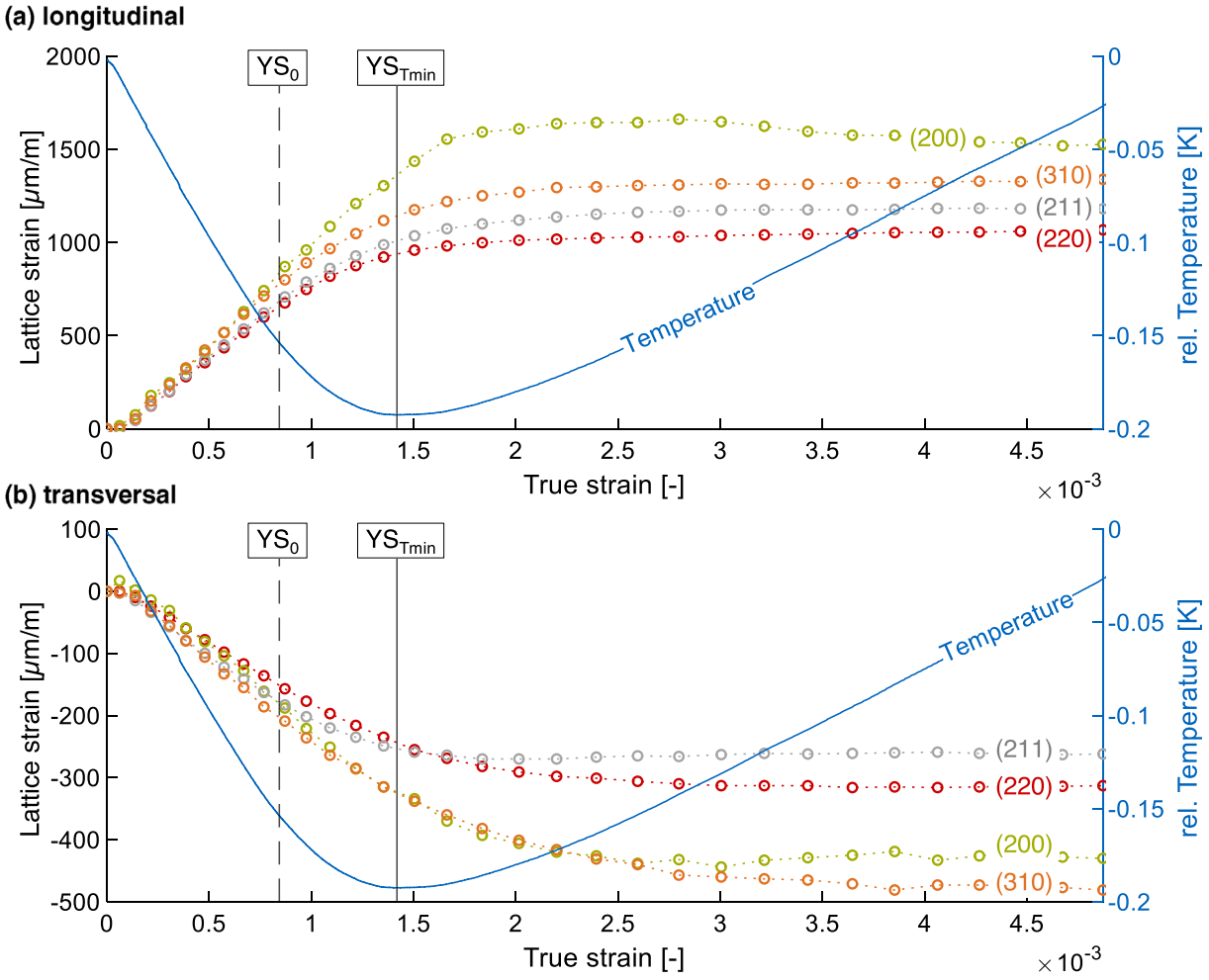

Fig. 8. Lattice strain versus macroscopic true strain for four lattice planes for the initial loading (HC260Y) in (a) longitudinal and (b) transversal direction to the tension direction and corresponding relative specimen temperature versus time curve (blue line). (For interpretation of the references to colour in this figure legend, the reader is referred to the web version of this article.)

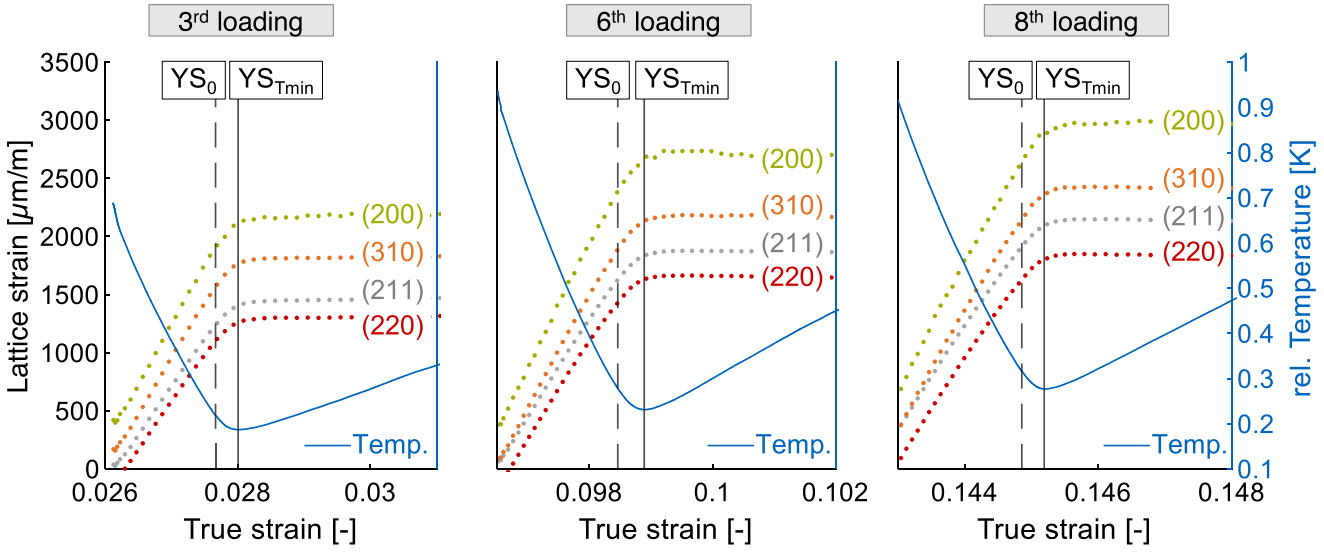

Fig. 9. Lattice strain versus macroscopic true strain for four lattice planes for three further loadings at different prestrains of the cyclic tensile test (HC260Y) and corresponding relative specimen temperature versus time curve (blue lines). (For interpretation of the references to colour in this figure legend, the reader is referred to the web version of this article.)

thermore, the elastic–plastic transition is not as smooth as it was for the initial loading. Plasticized grains can explain this, because slip systems have already been activated. Now the elastic–plastic transition is sharper, which is also evident from the temperature showing a more pronounced temperature minimum than it was for the initial loading (Fig. 8). The temperature minima of the specific loadings represent the point in time from which on the lattice planes no longer absorb any strain. This is the same for all loadings of the cyclic tensile test indicating that the temperature behavior can be correlated to the material behavior on a micro scale. This can be interpreted that the parameter YS_{Tmin} indicates the point in time at which the plastic deformation becomes predominant, but it is not the onset of yielding, as already assumed in [40]. The lattice strain behavior makes it evident that the grains start to plasticize beforehand.

The YS_0 parameter has been determined above, as indicating the onset of yielding. The parameter represents the upper linear elastic limit and the beginning of yielding, respectively. However, this does not imply that all lattice planes begin to plasticize at this point. On the contrary, it is clearly evident that the more elastic (200) plane is still in the elastic range at stresses higher than YS_0 (Fig. 8). Thus, comparison of the lattice strains in Fig. 8 reveals that the grains in different lattice orientations differ in their elastic–plastic transition. Deviation from linearity around YS_0 is visible for (310), (220) and (211) planes, indicating that yielding is initiated. The same trend is found in the transversal direction. For all subsequent loading cycles, the YS_0 represents the point in time when the lattice strains leave linearity as shown in Fig. 9. These findings emphasize that the parameter YS_0 actually does reflect the onset of yielding and is not chosen arbitrarily. Furthermore, the onset of yielding phase - or grain to grain yielding [70] - between YS_0 and YS_{Tmin} can be confirmed by the different behavior of the lattice planes. It is obvious that this behavior leads to the steady transition from elastic to elastic–plastic deformation.

6.2. Dislocation densities

In theory, the stress is increasing linearly during purely elastic deformation and no lattice defects are produced [5,71]. After the onset of yielding the number of crystal defects (i.e. dislocations) rises with increasing strain, which has been shown for example in [70]. Hence, the dislocation density seems to be a further appropriate value to describe the onset of yielding on the micro scale level. Furthermore, it is related to intra-grain micro strain and thus contributes only to the peak broadening and not to the peak shift like in the case of lattice strains stemming predominately from grain to grain (inter-granular) interactions. Fig. 10 shows the true stress versus the square root of the dislocation densities (SRD) for the initial, the 3rd, 6th and 8th loading in longitudinal (a) and transversal (b) direction. Again, the parameters YS_0 and YS_{Tmin}

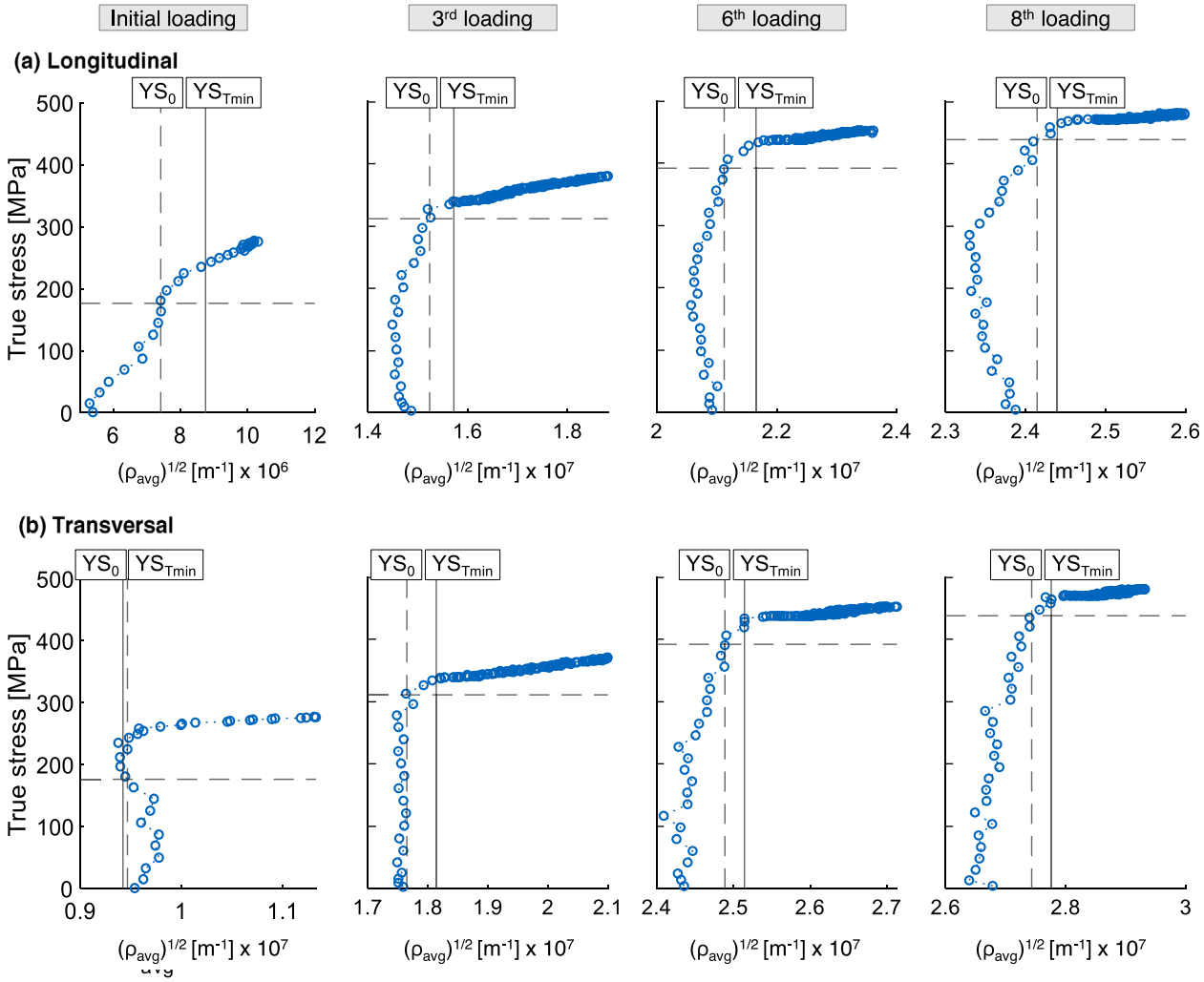

Fig. 10. True stress versus square root of dislocation density ρ_{avg} (HC260Y) in (a) longitudinal and (b) transversal direction. Shown are the initial, 3rd, 6th and 8th loading curves and the corresponding YS_0 and YS_{Tmin} of the cyclic tensile test.

are shown with vertical lines. To better identify the position of YS_0, a dashed horizontal line has been added for this value. Looking at the initial loading for longitudinal and transversal direction one can see that in longitudinal direction the SRD increases slightly from 0 MPa on and changes slope at a certain point. This change in slope is at the time of YS_0. Afterwards the SRD increases further until YS_{Tmin}. For the transversal direction, the SRD increases hardly with strongly increasing true stress. The parameters YS_0 and YS_{Tmin} are very close to each other and represent the point in time, where the SRD starts to increase. It must be noted here that due to the resolution of the experiment (see Fig. 6), which is similar to the initial peak width of the material, measurement inaccuracies in the intial loading are greater. This may explain the different behavior. However, material-specific reasons cannot be excluded. The 3rd, 6th and 8th loading show similar behavior for both evaluation directions. The transition from elastic to plastic behavior can be clearly seen in the plots. In addition, a certain jump in the SRD can be seen in this transition. Subsequently, the SRD and hence the dislocation density continues to increase steadily. The YS_0 is always in the range of this jump. The YS_{Tmin}, in turn, matches the point in time from which the SRD seem to rise in constant manner. A likely explanation is that the jump represents the activation of the slip system and YS_0 describes this state. The results of the lattice strains indicate a change in the microstructural behavior (grain to grain yielding) between YS_0 and YS_{Tmin}. The dislocation behavior shows again that there are changes in the microstructure in this area. It is a clear evidence that the two temperature parameters are related to and can characterize the onset of yielding as assumed on the basis of macroscopic data in [40]. The results and findings for all other loadings were found to be simliar.

Looking closely at Fig. 10 (a), it becomes evident that at higher prestrains, there is even a minimal decrease in density until YS_0 in longitudinal direction. These phenomena need to be investigated in more detail in future work with regard to anelastic material behavior, since the correlation between anelastic behavior and dislocation densities has already been stated in several studies [72–74]. There are also a number of micro-plasticity models that attempt to represent the nonlinear elastic material behavior as accurately as possible [75–77]. In these, nonlinearity is often associated with mobile dislocations [10]. Hence, these results and further evaluation can lead to a better material understanding and a possible improvement of the models.

7. Application of the YS_0 elasticity parameter

Young's modulus is one of the key influencing factors regarding springback, and therefore a reliable determination is crucial for precise springback prediction [44]. For several mechanical properties, such as the plastic yield curve, the value of Young's modulus is necessary [78]. Materials differ significantly in the elastic–plastic transition. As a result, no lower or upper limits for the determination in tensile tests are defined in the standards [12,13]. However, the choice of the limits strongly influences the result [15]. In [79] four different approaches for the determination of limits are suggested, but none has a real physical basis. With the parameters YS_0 and YS_{Tmin}, there are new possibilities describing the elastic–plastic material behavior. In the current study, it was shown that the parameter YS_0 reflects the onset of yielding and thus represents the upper elastic limit. Therefore, it seems obvious to use this limit as an upper limit for determination of Young's modulus. Fig. 11 (a) shows the true stress versus true strain curve of HC260Y steel for five loading–unloading cycles. The temperature elasticity parameters YS_0 and YS_{Tmin}, as well as the commonly used yield stress criterion at 0.2 % plastic strain ($YS_{0.2\%}$) are marked. For the

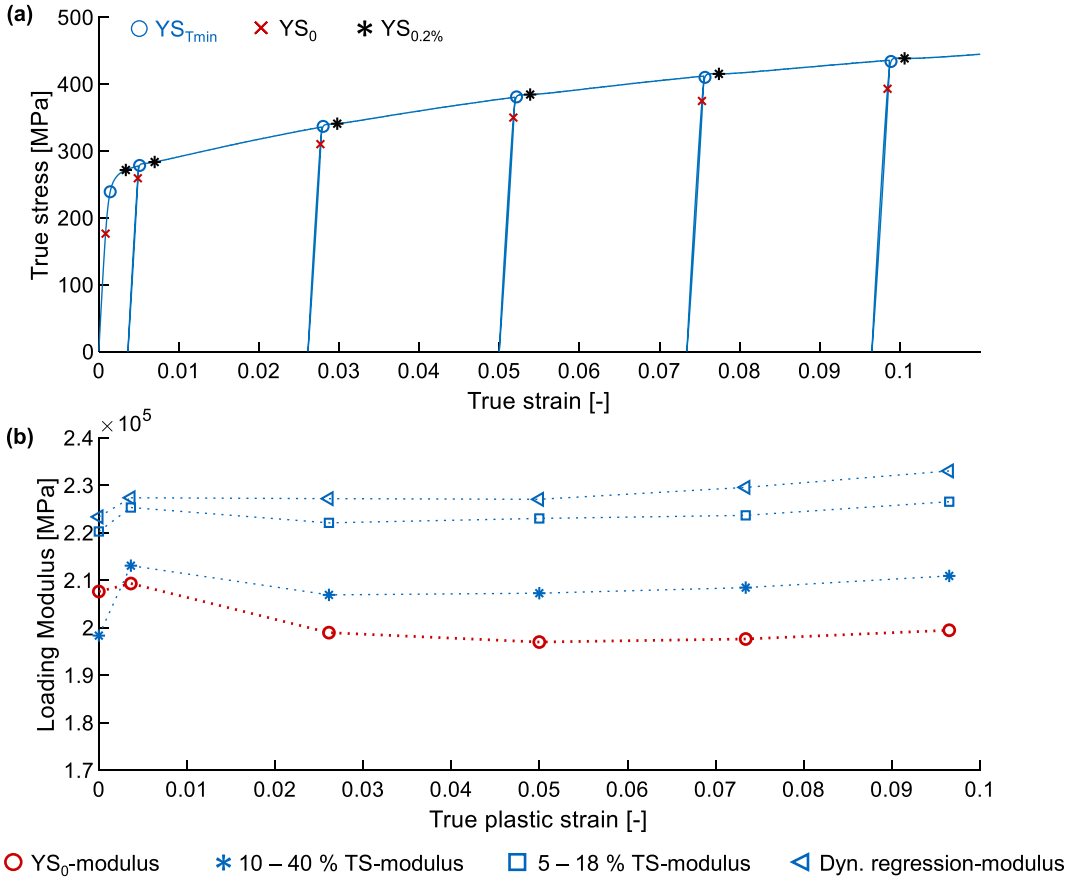

Fig. 11. (a) Comparison of the parameters YS_{Tmin}, YS_0 and $YS_{0.2\%}$; (b) Comparison of strain-dependency of the loading modulus based on different determination methods.

determination $YS_{0.2\%}$ fitting of the elastic slope is necessary [12], which is a clear disadvantage compared to the YS_{Tmin}. In the following, the YS_0-modulus is chosen as a upper limit for the linear fit of the $YS_{0.2\%}$ determination. The stress at 5 % of the tensile strength was chosen as the lower limit, as suggested in [79], to overcome possible acceleration effects in the beginning of the loading. Finally, the loading modulus is determined using a simple linear regression between this lower limit and the specific YS_0 value for each loading. Clearly, $YS_{0.2\%}$ is higher in the stress–strain curve than the YS_0 and the YS_{Tmin}, which is obvious, because YS_0 is at zero plastic strain and the YS_{Tmin} is at a very early state of yielding. Fig. 11 (b) shows the loading moduli of the first six loadings determined by different evaluation approaches. It has to be stated that the focus of the experiment was not the determination of Young's modulus, so the experiment does not meet the requirements of the standards for Young's modulus determination [12,13], but it is appropriate for an exemplary comparison. It is evident that the resulting loading moduli significantly differ. Compared are the results from a dynamical regression method, which analyzes the loading curve using different numbers of data points and selects the area of least error in the fit as the modulus. Furthermore, results from two determination approaches are shown, which are based on lower and upper limits dependent on the tensile strength. One is based on the linear regression between 5 % and 18 % of the tensile strength, as suggested by [79]. For the other one the limit were changed to 10 % and 40 %, respectively. Fig. 11 (b) indicated clearly the dependency of the elastic modulus on the determination method. The HC260Y steel has a smooth elastic–plastic transition, which on closer inspection is not linear. Because of the nonlinear convex shape of the loading curve, determination methods using the lower area of the loading curve provide higher values. On the other hand, the moduli derived based on the YS_0 approach show reasonable results with an initial modulus close to 210 GPa with a slight decrease with increasing prestrain. This behavior is well known from literature [80,81]. The advantage compared to the more standard methods is that the upper limit was not found or chosen arbitrarily, but is based on a material-dependent relationship. With regard to reliable results and their simplicity in determination, the YS_0-modulus is more robust and therefore to be preferred.

8. Conclusion

Within this study, an experimental setup is introduced, which allows to measure the specimen temperature during tensile tests with high precision and synchronously track diffraction data with synchrotron radiation. Thus, the thermoelastic effect and its relation to the onset of yielding can be investigated on microstructural level and compared to macroscopic material behavior. This investigation provides the basis for using the thermoelastic effect, i.e. by using the minimum in the temperature curve as a material parameter. Furthermore, an evaluation method using the temperature gradient is comprehensibly evaluated and qualified. The focus of the study is to show the link between the thermoelastic effect and the onset of yielding in detail elucidating the material dependency of the yield stress at temperature minimum (YS_{Tmin}) and maximum yield stress at zero plastic strain (YS_0) parameters. This was possible by in-situ synchrotron diffraction experiments. Finally, with the determination of the elastic loading modulus, a possible application for the parameters was shown and indicate that modulus determination based on YS_0 would be preferably. The findings of the work can be summarized as follows:

- In-situ diffraction experiments substantiate the relation of the temperature minimum and the onset of yielding. Correlating the measured lattice strains with the temperature signal showed that the material is globally in the elastic–plastic deformation state at temperature minimum.
- It was demonstrated that an additional yield stress parameter YS_0 can be determined using the first derivative of the temperature signal and it represents the upper linear elastic stress limit.
- Comparison of the dislocation density evolution in the material with the temperature behavior strongly corroborate the findings from the stain measurements. The YS_0 reflected the point in time where the dislocation density starts to increase rapidly. The dislocation behavior also showed that their behavior changed at the time of both parameters YS_0 and YS_{Tmin} respectively.
- Based on the parameter YS_0, a method to determine the elastic loading modulus was introduced. Taking the YS_0 value as the upper limit for the determination of Young's modulus has the advantage that it is a material-dependent value and can be determined by a simple macroscopic tensile test. In comparison with other determination methods, this method is less sensitive to the choice of boundary conditions.

In summary, the YS_{Tmin} seems to be a suitable material parameter and in contrast to the widely used $YS_{0.2\%}$, it is a directly measurable value, and less error-prone. Furthermore, it was shown that it is significantly closer to the onset of yielding than the $YS_{0.2\%}$. The introduced temperature measurement provides great potential for material characterization, as shown by the parameter YS_0. In a next step, the impact of this method on existing material models must be investigated and it might be used to expand and improve some of those models.

Declaration of Competing Interest

The authors declare that they have no known competing financial interests or personal relationships that could have appeared to influence the work reported in this paper.

Acknowledgements

The author would like to thank the German Research Foundation (DFG) for the financial support under the grant number 429432653. Furthermore, the authors would like to thank the team of Hereon Geesthacht for the measurement opportunity at the side station of the HEMS beamline at PETRA III synchrotron (DESY). In addition, Professor Susumu Takahashi is thanked for providing measurement equipment.

Data Availability

The raw/processed data required to reproduce these findings cannot be shared at this time as the data also forms part of an ongoing study.

References

[1] K. Roll, T. Lemke, K. Wiegand, Possibilities and Strategies for Simulations and Compensation for Springback, American Institute of Physics, 2005.
[2] F. Morestin, M. Boivin, On the necessity of taking into account the variation in the Young modulus with plastic strain in elastic-plastic software, Nucl. Eng. and Design 162 (1) (1996) 107–116.
[3] M.O. Andar, T. Kuwabara, S. Yonemura, A. Uenishi, Elastic-Plastic and Inelastic Characteristics of High Strength Steel Sheets under Biaxial Loading and Unloading, ISIJ Int. 50 (4) (2010) 613–619.
[4] F. Yoshida, T. Uemori, K. Fujiwara, Elastic–plastic behavior of steel sheets under in-plane cyclic tension–compression at large strain, Int. J. Plast. 18 (5-6) (2002) 633–659.

[5] R. Hooke, Lectures de Potentia Restitutiva, Or, Of Spring: Explaining the Power of Springing Bodies to which are Added Some Collections Viz. a Description of Dr. Pappins Wind-fountain and Force-pump, Mr. Young's Observation Concerning Natural Fountains, Some Oth, John Martyn (1678.).
[6] J.R. Davis, Tensile testing, 2nd ed., ASM International, Materials Park, Ohio, 2010.
[7] D. Li, R.H. Wagoner, The nature of yielding and anelasticity in metals, Acta Mater. 206 (2021) 116625.
[8] H. Kim, C. Kim, F. Barlat, E. Pavlina, M.-G. Lee, Nonlinear elastic behaviors of low and high strength steels in unloading and reloading, Mat. Sc. and Eng.: A 562 (2013) 161–171.
[9] J. Mendiguren, F. Cortés, X. Gómez, L. Galdos, Elastic behaviour characterisation of TRIP 700 steel by means of loading–unloading tests, Mat. Sc. and Eng.: A 634 (2015) 147–152.
[10] R.M. Cleveland, A.K. Ghosh, Inelastic effects on springback in metals, Int. J. Plast. 18 (5-6) (2002) 769–785.
[11] C.E. Bottani, G. Caglioti, Thermal emission: A probe to identify the critical point of the elastoplastic transition, Materials Letters 1 (1982) 119–121.
[12] DIN Deutsches Institut für Normung e. V., Metallic materials – Tensile testing: Part 1: Method of test at room temperature(DIN EN ISO 6892-1), Berlin, Beuth Verlag GmbH, 2020.
[13] ASTM, Test Method for Youngs Modulus, Tangent Modulus, and Chord Modulus(E 111-17), West Conshohocken, PA, ASTM International, 10.1520/E0111-17.
[14] Deutsches Institut für Normung e.V., Metallische Werkstoffe - Zugversuch - Teil 1: Prüfverfahren bei Raumtemperatur (ISO 6892-1:2016);(ISO 6892-1:2016), Berlin, Beuth Verlag GmbH, 2017.
[15] S. Ledworuski, M. Ell, H.-J. Kühn, Den Elastizitätsmodul sicher bestimmen, Materials Testing 42 (2000) 109–113.
[16] G. Sallat, Theoretische und experimentelle Untersuchungen zum Fliessverhalten von Blechen im Zweiachsigen. Dissertation, Chemnitz, 1988.
[17] W. Weber, Ueber die specifische Wärme fester Körper, insbesondere der Metalle, Ann. Phys. Chem. 96 (10) (1830) 177–213.
[18] W. Thomson, XV.— On the Dynamical Theory of Heat, with numerical results deduced from Mr Joule's Equivalent of a Thermal Unit, and M, Regnault's Observations on Steam, Trans. R. Soc. Edinb. 20 (2) (1853) 261–288.
[19] J.P. Joule, W. Thomson, LXXVI. On the thermal effects experienced by air in rushing through small apertures, The London, Edinburgh, Dublin Philosophical Magazine J. Sci. 4 (28) (1852) 481–492.
[20] J.M. Dulieu-Barton, Introduction to thermoelastic stress analysis, Strain 35 (2) (1999) 35–39.
[21] H.W. Lord, Y. Shulman, A generalized dynamical theory of thermoelasticity, J. Mech. Phys. Solids 15 (5) (1967) 299–309.
[22] E. Doege, B.-A. Behrens, Handbuch Umformtechnik: Grundlagen, Technologien, Maschinen, 2nd ed., Springer-Verlag, s.l., 2010.
[23] K.N. Pandey, S. Chand, Deformation based temperature rise: a review, International Journal of Pressure Vessels and Piping 80 (10) (2003) 673–687.
[24] A.K. Wong, G.C. Kirby, A hybrid numerical/experimental technique for determining the heat dissipated during low cycle fatigue, Engineering Fracture Mechanics 37 (3) (1990) 493–504.
[25] A.T. Zehnder, A.J. Rosakis, On the temperature distribution at the vicinity of dynamically propagating cracks in 4340 steel, Journal of the Mechanics and Physics of Solids 39 (3) (1991) 385–415.
[26] K.T. Compton, D.B. Webster., Temperature Changes Accompanying the Adiabatic Compression of Steel, Phys. Rev. 5 (2) (1915) 159–166.
[27] R. Rocca, M.B. Bever, Bever, The thermoelastic effect in iron and nickel as a function of temperature, JOM 2 (2) (1950) 327–333.
[28] M.A. Biot, Theory of Elasticity and Consolidation for a Porous Anisotropic Solid, J. Appl. Phys. 26 (2) (1955) 182–185.
[29] M.A. Biot, Thermoelasticity and Irreversible Thermodynamics, J. Appl. Phys. 27 (3) (1956) 240–253.
[30] W.N. Sharpe, Springer handbook of experimental solid mechanics, Springer, New York, 2008.
[31] H.-T. Lee, J.-C. Chen, Temperature effect induced by uniaxial tensile loading, J Mater Sci 26 (21) (1991) 5685–5692.
[32] M.H. Belgen, Structural Stress Measurements with an Infrared Radiometer, ISA Trans 6 (1967) 49–53.
[33] W. Oliferuk, M. Maj, R. Litwinko, L. Urbański, Thermomechanical coupling in the elastic regime and elasto-plastic transition during tension of austenitic steel, titanium and aluminium alloy at strain rates from 10–4 to 10–1 s−1, Eur. J. Mech. - A/Solids 35 (2012) 111–118.
[34] A. Lipski, Change of specimen temperature during the monotonic tensile test and correlation between the yield strength and thermoelasto-plastic limit stress on the example of aluminum alloys, Materials 14 (2021) 13.
[35] P. Patil, K. Thiyagarajan, R.V. Prakash, K. Balasubramaniam, Damage characterization in SS 304 due to monotonic loading using infrared thermography, Int. J. Adv. Manuf. Technol. 37 (2009) 853.
[36] R.V. Prakash, T. Pravin, T. Kathirvel, K. Balasubramaniam, Thermo-mechanical measurement of elasto-plastic transitions during cyclic loading, Theoretical Appl. Fracture Mech. 56 (1) (2011) 1–6.
[37] C. Chandraprakash, C.V. Krishnamurthy, K. Balasubramaniam, Thermomechanical Phenomenon: A Non-destructive Evaluation Perspective, Trans Indian Inst Met 72 (11) (2019) 2905–2915.
[38] I. Jandrlić, S. Rešković, F. Vodopivec, P. Lava, Dependence of thermoelastic effect on volume change by elastic deformation, Met. Mater. Int. 22 (3) (2016) 407–412.
[39] D. Jocham, S. Vitzthum, T. Susumu, W. Annika, V. Wolfram, Yield locus determination of DX56 on a testing apparatus with link mechanism using thermoelectrical effect and equivalent plastic work, 9th Forming Technology, Forum (2016).
[40] S. Vitzthum, C. Hartmann, M. Eder, W. Volk, Temperature-based determination of the onset of yielding using a new clip-on device for tensile tests, Procedia Manufacturing 29 (2019) 490–497.
[41] X.X. Zhang, H. Andrä, S. Harjo, W. Gong, T. Kawasaki, A. Lutz, M. Lahres, Quantifying internal strains, stresses, and dislocation density in additively manufactured AlSi10Mg during loading-unloading-reloading deformation, Mater. Des. 198 (2021) 109339.
[42] X.X. Zhang, A. Lutz, H. Andrä, M. Lahres, W.M. Gan, E. Maawad, C. Emmelmann, Evolution of microscopic strains, stresses, and dislocation density during in-situ tensile loading of additively manufactured AlSi10Mg alloy, Int. J. Plast. 139 (2021) 102946.
[43] J. Macchi, S. Gaudez, G. Geandier, J. Teixeira, S. Denis, F. Bonnet, S.Y.P. Allain, Dislocation densities in a low-carbon steel during martensite transformation determined by in situ high energy X-Ray diffraction, Mat. Sc. Eng.: A 800 (2021) 140249.
[44] R.H. Wagoner, H. Lim, M.-G. Lee, Advanced Issues in springback, Int. J. Plast. 45 (2013) 3–20.
[45] W. Volk, P. Groche, A. Brosius, A. Ghiotti, B.L. Kinsey, M. Liewald, L. Madej, J. Min, J. Yanagimoto, Models and modelling for process limits in metal forming, CIRP Ann. 68 (2) (2019) 775–798.
[46] M. Cardona, P. Fulde, H.-J. Queisser, G. Benedek, H. Bilz, R. Zeyher, Statics and Dynamics of Nonlinear Systems, Springer, Berlin Heidelberg, Berlin, Heidelberg, 1983.
[47] C.E. Bottani, G. Caglioti, Thermoelastic Instabilities in Metals, Phys. Scr. T T1 (1982) 65–70.
[48] P. Heinz, Thermoelasticity, Springer Vienna, Vienna, 1976.
[49] M.B. Bever, D.L. Holt, A.L. Titchener, The stored energy of cold work, Prog. Mater. Sci. 17 (1973) 5–177.
[50] B.A. Boley, J.H. Weiner, Theory of Thermal Stresses, Dover Publications, Newburyport, 2012.
[51] D. Banabic, K. Pöhlandt, Formability of metallic materials: Plastic anisotropy, formability testing, forming limits, Springer, Berlin, Heidelberg, 2000.
[52] W. Volk, P. Hora, New algorithm for a robust user-independent evaluation of beginning instability for the experimental FLC determination, Int J Mater Form 4 (3) (2011) 339–346.
[53] A.P. Hammersley, FIT2D: An Introduction and Overview, ESRF Internal Report (1997).
[54] M. Hoelzel, W.M. Gan, M. Hofmann, C. Randau, G. Seidl, P.h. Jüttner, W.W. Schmahl, Rotatable multifunctional load frames for neutron diffractometers at FRM II—design, specifications and applications, Nuclear Instruments and Methods in Physics Research Section A: Accelerators, Spectrometers, Detectors and Associated Equipment 711 (2013) 101–105.
[55] W.H. Bragg, W.L. Bragg, The Reflection of X-rays by Crystals, Proc. Royal Soc. A: Math., Phys. and Eng. Sc. 88 (1913) 428–438.
[56] A.P. Stebner, D.W. Brown, L.C. Brinson, Young's modulus evolution and texture-based elastic–inelastic strain partitioning during large uniaxial deformations of monoclinic nickel–titanium, Acta Mater. 61 (6) (2013) 1944–1956.
[57] Z.Y. Zhong, H.-G. Brokmeier, W.M. Gan, E. Maawad, B. Schwebke, N. Schell, Dislocation density evolution of AA 7020–T6 investigated by in-situ synchrotron diffraction under tensile load, Mat. Charact. 108 (2015) 124–131.
[58] E. Mittemeijer, U.J. Welzel, (Keine Angabe), Diffraction stress analysis of macroscopically elastically anisotropic specimens: On the concepts of diffraction elastic constants and stress factors, Journal of Applied Physics 93 (2003) 9001–9011.
[59] P. Scardi, M. Leoni, R. Delhez, Line broadening analysis using integral breadth methods: a critical review, J Appl Crystallogr 37 (3) (2004) 381–390.
[60] Y. Zhao, J. Zhang, Microstrain and grain-size analysis from diffraction peak width and graphical derivation of high-pressure thermomechanics, J Appl Crystallogr 41 (6) (2008) 1095–1108.
[61] C. Suryanarayana, M.G. Norton (Eds.), X-Ray Diffraction, Springer US, Boston, MA, 1998.
[62] T. Ungár, A. Borbély, The effect of dislocation contrast on x-ray line broadening: A new approach to line profile analysis, Appl. Phys. Lett. 69 (1996) 3173–3175.
[63] S. Das Bakshi, D. Sinha, S. Ghosh Chowdhury, Anisotropic broadening of XRD peaks of α′-Fe: Williamson-Hall and Warren-Averbach analysis using full width at half maximum (FWHM) and integral breadth (IB), Mat. Charact. 142 (2018) 144–153.
[64] P. Bindu, S. Thomas, Estimation of lattice strain in ZnO nanoparticles: X-ray peak profile analysis, J Theor Appl Phys 8 (2014) 123–134.
[65] J. Lu (Ed.), Handbook of measurement of residual stresses, Fairmont Press, Lilburn, GA, 1996.
[66] G.K. Williamson, W.H. Hall, X-ray line broadening from filed aluminium and wolfram, Acta, Metal. 1 (1) (1953) 22–31.
[67] R. Delhez, T.H. de Keijser, E.J. Mittemeijer, Determination of crystallite size and lattice distortions through X-ray diffraction line profile analysisBestimmung von Kristallitgrößen und Gitterverzerrungen durch Röntgenbeugungs-Linienprofilanalyse: Recipes, methods and comments, Z. Anal. Chem. 312 (1) (1982) 1–16.
[68] F. Christien, M.T.F. Telling, K.S. Knight, R. Le Gall, A method for the monitoring of metal recrystallization based on the in-situ measurement of the elastic

energy release using neutron diffraction, Review of Scientific Instruments 86 (2015) 53901.
[69] G.K. Williamson, R.E. Smallman, Dislocation densities in some annealed and cold-worked metals from measurements on the X-ray debye-scherrer spectrum, Philosophical Magazine 1 (1) (1956) 34–46.
[70] Y. Tomota, P. Lukas, S. Harjo, J.-H. Park, N. Tsuchida, D. Neov, In situ neutron diffraction study of IF and ultra low carbon steels upon tensile deformation, Acta Mater. 51 (3) (2003) 819–830.
[71] D. Banabic (Ed.), Sheet Metal Forming Processes, Springer Berlin Heidelberg, Berlin, Heidelberg, 2010.
[72] A. Kupke, L. Madej, P.D. Hodgson, M. Weiss, Experimental in-situ verification of the unloading mechanics of dual phase steels, Mat. Sc. and Eng.: A 760 (2019) 134–140.
[73] A. Torkabadi, E.S. Perdahcıoğlu, V.T. Meinders, A.H. van den Boogaard, On the nonlinear anelastic behavior of AHSS, International Journal of Solids and Structures 151 (2018) 2–8.
[74] Z. Arechabaleta, P. van Liempt, J. Sietsma, Quantification of dislocation structures from anelastic deformation behaviour, Acta Mater. 115 (2016) 314–323.
[75] L. Sun, R.H. Wagoner, Complex unloading behavior: Nature of the deformation and its consistent constitutive representation, Int. J. Plast. 27 (2011) 1126–1144.
[76] F. Yoshida, T. Amaishi, Model for description of nonlinear unloading-reloading stress-strain response with special reference to plastic-strain dependent chord modulus, Int. J. Plast. 130 (2020) 102708.
[77] J. Lee, J.-Y. Lee, F. Barlat, R.H. Wagoner, K. Chung, M.-G. Lee, Extension of quasi-plastic–elastic approach to incorporate complex plastic flow behavior – application to springback of advanced high-strength steels, Int. J. Plast. 45 (2013) 140–159.
[78] S. Suttner, M. Merklein, A new approach for the determination of the linear elastic modulus from uniaxial tensile tests of sheet metals, J. Mater. Process. Technol. 241 (2017) 64–72.
[79] H.M. Sonne, Bestimmung des Elastizitäsmoduls im Zugversuch, Bad Nauheim, Vortrags- und Diskussionstagung, 1999, pp. 219–230.
[80] S.F. Lajarin, C.P. Nikhare, P.V.P. Marcondes, Dependence of plastic strain and microstructure on elastic modulus reduction in advanced high-strength steels, J Braz. Soc. Mech. Sci. Eng. 40 (2018) 129.
[81] Z. Chen, U. Gandhi, J. Lee, R.H. Wagoner, Variation and consistency of Young's modulus in steel, J. Mat. Proc. Techn. 227 (2016) 227–243.